

Efficient catalytic effect of CuO nanostructures on the degradation of organic dyes

Siama Zaman, Ahmed Zainelabdin, Gul Amin, Omer Nour and Magnus Willander

Linköping University Post Print

N.B.: When citing this work, cite the original article.

Original Publication:

Siama Zaman, Ahmed Zainelabdin, Gul Amin, Omer Nour and Magnus Willander, Efficient catalytic effect of CuO nanostructures on the degradation of organic dyes, 2012, Journal of Physics and Chemistry of Solids, (73), 11, 1320-1325.

<http://dx.doi.org/10.1016/j.jpcs.2012.07.005>

Copyright: Elsevier

<http://www.elsevier.com/>

Postprint available at: Linköping University Electronic Press

<http://urn.kb.se/resolve?urn=urn:nbn:se:liu:diva-81427>

Efficient catalytic effect of CuO nanostructures on the degradation of organic dyes

S. Zaman*, A. Zainelabdin, G. Amin, O. Nur and M. Willander

Department of Science and Technology, Campus Norrköping,

Linköping University, SE-60174 Norrköping, Sweden

***Corresponding Author:** saiza@itn.liu.se

ABSTRACT

An efficient catalytic effect of petals and flowers like CuO nanostructures (NSs) on the degradation of two organic dyes, methylene blue (MB) and rhodamine B (RB) were investigated. The highest degradation of 95% in CuO petals and 72 % in flowers for MB is observed in 24 h. For RB, the degradation was 85 % and 80 % in petals and flowers, respectively for 5 h. It was observed that CuO petals appeared to be more active than flowers for degradation of both dyes associated to high specific surface area. The petals and flower like CuO NSs were synthesized using the chemical bath method at 90 °C. The grown CuO NSs were characterized using scanning electron microscopy (SEM), high resolution transmission electron microscopy (HRTEM), and X-ray diffraction (XRD).

Keywords: CuO flowers, CuO petals, catalytic effect

1. Introduction

In the last few years, synthesis of metal oxide nanostructures with desired architecture has received considerable attention due to their unique properties and potential for many applications [1, 2]. Among metal oxides, cupric oxide (CuO) is a p-type semiconductor with a narrow bandgap of 1.2 eV [3]. The synthesis and application of CuO nanostructures are of practical and fundamental importance. CuO is used in various applications like gas sensors [4], solar energy conversion [5], electrode material in lithium ion batteries [6], as field emitter [7], and as a heterogeneous catalyst [8]. Due to the versatile properties and diverse applications, various kinds of CuO nanostructures and microstructures e.g. nanorods, nanosheets, and nanodendrites as well as honeycomb-like, urchin-like and dumbbell-like structures [9-12] have been synthesized using a variety of fabrication techniques including the chemical bath method, sol-gel method, gas phase oxidation, micro-emulsion, and many other techniques [13-16]. Among these techniques the wet chemical growth method is widely used due to its low temperature, easiness, and cost efficient nature compared to other fabrication techniques.

Industrial dyestuff comprises one of the largest groups of organic compounds that cause discolouration of water and cause great loss of aquatic life. The removal of these colors and other organic materials is a priority for ensuring a safe and clean environment [17]. Advanced oxidation processes (AOPs) have been used during the last decade to degrade dyes in aqueous media without the formation of hazardous by-products [18]. AOPs are based on the generation of very reactive species such as hydroxyl radicals (OH^\cdot) that oxidize a broad range of pollutants very quickly. But the high operating costs of these processes are their main disadvantage [19]. Irradiation sources have a crucial role in enhancing the activity of catalysts, and UV radiation sources are widely used but they are also expensive and polluting [20].

CuO is one of the most important catalysts, and is commonly used as environmental catalyst. Previous studies indicate that the catalytic reaction is apparently a structure sensitive process and the oxygen surface lattice of CuO is involved in the reaction [21]. The catalytic reactivity of CuO nanostructures depends on the shape and the exposed crystal planes. Hence the architectural shape-controlled synthesis of CuO structures may be helpful for designing novel structures with desired improved performance [22].

Here, the catalytic activities of CuO nanostructures (NSs) were examined through the degradation of rhodamine B (RB) and methylene blue (MB) in the presence of hydrogen peroxide H_2O_2 . The CuO petals demonstrated the highest catalytic properties for the degradation of RB and MB in short time. The catalytic performance of CuO petals and flowers studied here suggests that these NSs are efficiently used to degrade the RB and MB.

2. Experimental Section

2.1 Synthesis of CuO nanostructures

Copper nitrate trihydrate ($\text{Cu}(\text{NO}_3)_2 \cdot 3\text{H}_2\text{O}$), hexamethylenetetramine (HMT), sodium hydroxide (NaOH), methylene blue (MB), rhodamine B (RB), and commercial copper oxide (CuO) powder were purchased from Sigma Aldrich. All chemicals used were of analytical grade and used without further purification.

For the synthesis of flowers and petals like CuO nanostructures a modified procedure of Ref. [23] was used, in which a 5 mM of copper nitrate trihydrate and 1 mM of HMT were mixed in de-ionized (DI) water and the solution was stirred for 5 min. Then the reaction vessel was loaded in a laboratory oven at 90 °C for 4-5 h for growing the CuO flowers. After the growth CuO flowers powder was collected and washed thoroughly with deionized water and left to dry at room temperature. While for the growth of the CuO petals a 1 mL of NaOH (30 %) was added to the aqueous solution of the copper nitrate and the HMT.

The catalytic activities of as grown NSs were investigated using an aqueous solution of methylene blue (MB) and rhodamine B (RB). The typical catalytic reactions were carried out at room temperature in a sealed glass beaker containing 100 mL of an aqueous solution of MB or RB (0.2 g/L). A 20 mL of hydrogen peroxide (H_2O_2 30 wt%) and 20 mg of CuO NSs were added to the dye solution, and the mixture was allowed to react for 30 min to reach equilibrium. After a given time interval, 2 mL of solution was withdrawn and the UV-visible absorption spectrum was measured.

2.2 Characterization

The morphology of the as grown CuO NSs was examined using field emission scanning electron microscopy (FESEM) complemented by transmission electron microscopy (TEM) measurements. The crystal phase and crystallinity were analysed by X-ray diffractometer (XRD). A UV-visible absorption spectrometer was used to determine the absorption of the degraded solution of MB and RB. Nitrogen adsorption measurement was performed by Autosorb-1Q Quantachrome Instrument volumetric adsorption analyzer to determine the specific surface area of the CuO NSs.

3. Results and discussion

3.1 The morphology and structure of the CuO nanostructures

The shape and morphology of the flowers-like and petals-like CuO NSs are shown in the SEM micrographs of figure 1. The low magnification image shows that the CuO flowers are uniformly covering the substrate figure 1a. A high magnification SEM image of the CuO flowers is shown in figure 1b reveals that they are composed of several layers of leaf-like nanostructures. These leaves have wider bases and very sharp tips of about 10–20 nm and diverging outside as shown in the inset of figure 1a. The average diameter of the flower is about ~ 4 - 5 μ m and the diameter of a single leaf is about 400 - 500 nm. CuO petals also show a good substrate coverage over the substrate as can be seen in the low magnification SEM image of figure 1c, while the high magnification image shows that one petal consists of many interpenetrated sheet-like nanostructures.

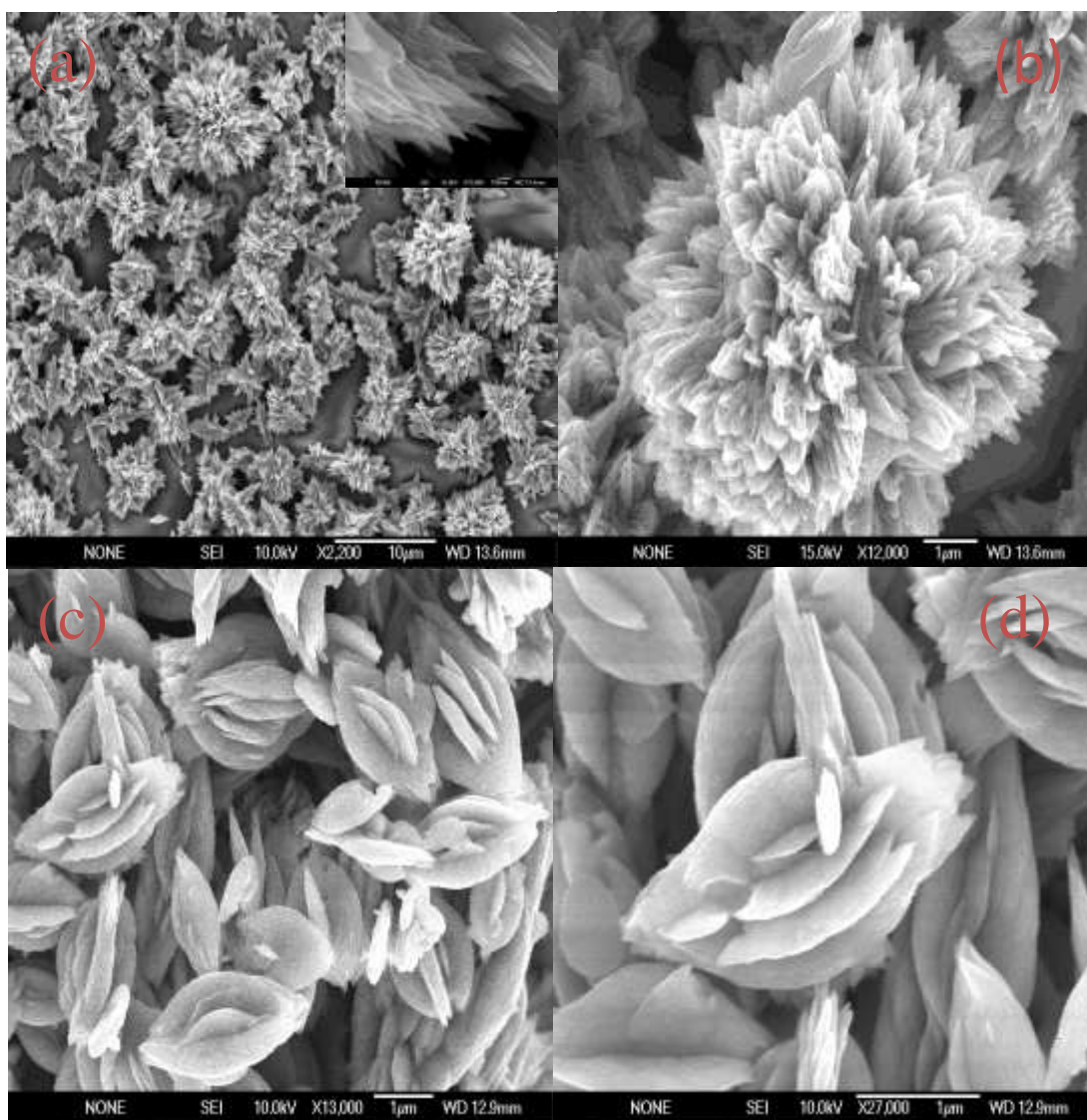


Figure 1: (a) Typical SEM of low and (b) high magnification image of CuO flowers and inset of (a) shows the very sharp tips of CuO flowers. (c) and (d) Low and high magnification of CuO petals, respectively.

Figure 2a shows a TEM image of a single CuO flower, and it can be clearly seen that the flower is composed of layered leaf like structures which is consistent with the SEM observations.

The central part of the grown CuO flower looks bulky and exhibit less structural defects as compared to the edge part of the flower. The HRTEM image taken from the edges of the CuO flower is shown in the inset of figure 2a also confirms this finding and shows that there are large structural defects such as screw dislocations in this region. Figure 2b show the TEM image of the CuO petals which reveals a well-defined structure with accumulation of an interpenetrating sheet-like nanostructure. The typical length and width of the petals are in the ranges 1.5–2 μm and 300–400 nm, respectively. The growth of the CuO petals along the [010] planes is faster compared to the [100] plane. Among the three planes [001], [010] and [100] the most thermodynamically stable plane is the [001] while the least stable one is the [010] due to the highest and lowest density of copper atoms on these planes. Therefore, preferential aggregated growth takes place along the [010] which has the highest reactivity [24]. HRTEM images of the corresponding CuO petals are shown in the inset of figure 2. The straight and parallel lattice fringes reveal that the CuO petals are of good crystalline nature. The 'd' spacing between the crystallographic plane is 0.232 nm, corresponding to the (110) lattice fringe of monoclinic CuO. The selected area electron diffraction (SAED) pattern shows that the CuO petals have a single crystalline structure. As evident that the SAED spots are slightly stretched an indication that the petals are composed of large density of nanocrystals with limited orientation deviation. Interestingly petals are composed of nanowires (NWs) and these NWs are assembling through oriented attachment to form nanocrystals. According to the oriented attachment growth model of NSs, we expect that the CuO petals NSs were formed by NWs aggregation [24, 25].

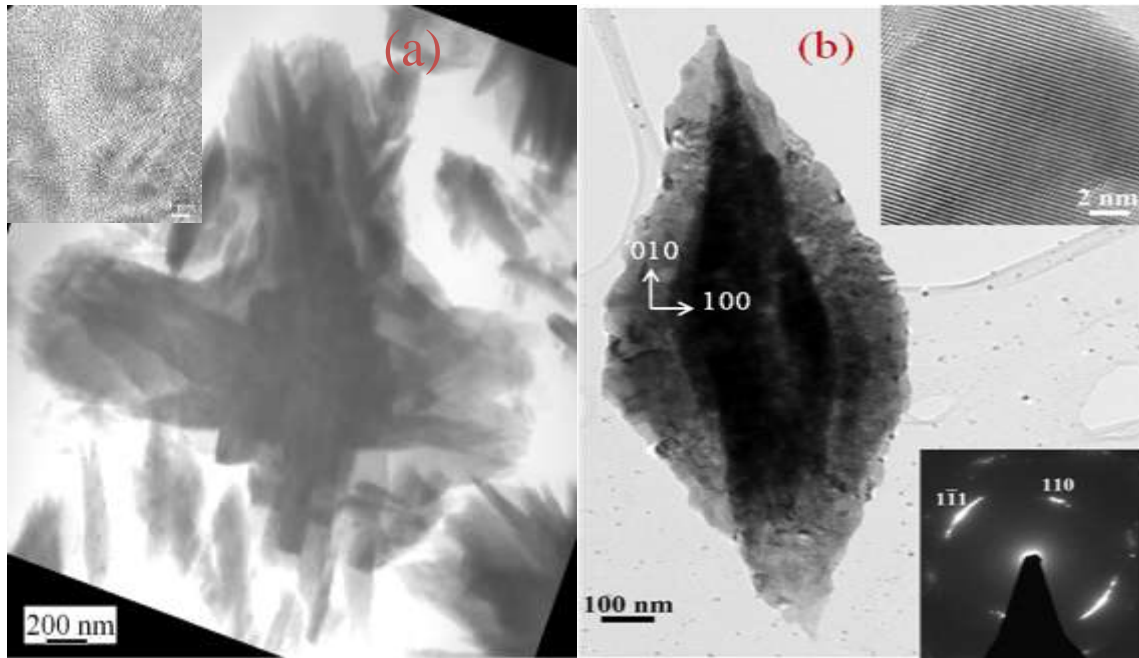


Figure 2: TEM and HRTEM images of (a) CuO flowers and (b) CuO petals and inset are a SAED pattern of the petals structure.

The crystallinity of the grown CuO flowers and petals was also confirmed by using XRD as shown in figure 3. The major peaks at 2θ values of 32.5° , 35.5° , and 38.5° , which are indexed to the (110), (11-1)-(002), and (111)-(200) planes, respectively, are consistent with the JCPDS (card no. 05-661) and ascribed to the pure monoclinic CuO crystal phase. Except for CuO peaks, no extra impurity peaks such as Cu or $\text{Cu}(\text{OH})_2$ were observed.

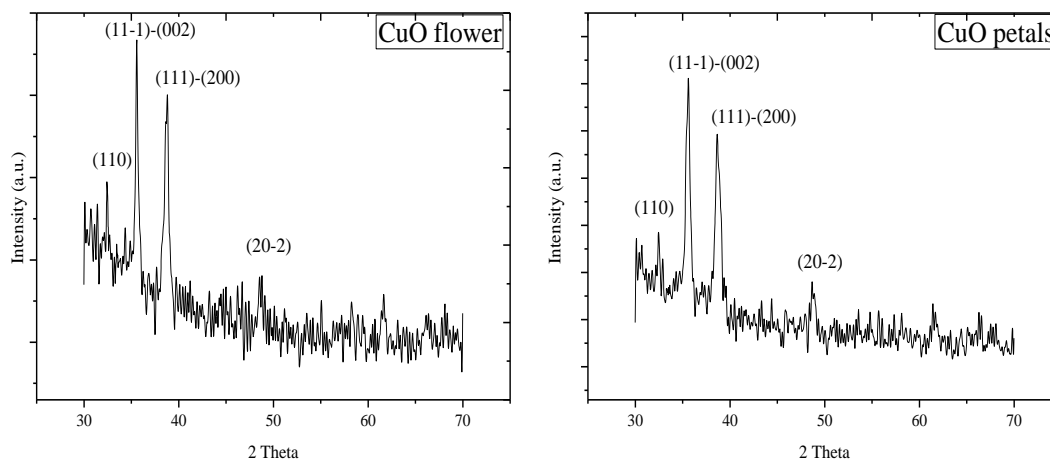


Figure 3: X-ray diffraction (XRD) pattern of the CuO flowers and petals nanostructures. Both are well crystalline and have monoclinic structure.

3.2 Catalytic effect of CuO nanostructures

3.2.1 Catalytic activity in rhodamine B

The catalytic activity of flowers-like and petals-like CuO NSs was investigated for the degradation of rhodamine B in the presence of H_2O_2 at room temperature, while examining RB absorption spectrum using the UV-visible spectroscopy. The structure of RB is shown in figure 4, with absorption peak of at ~ 554 nm, which was carefully monitored at various time intervals [26]. As can be seen in figure 5e, in the absence of CuO NSs, RB is barely degraded when only H_2O_2 is added to the RB aqueous solution: it is only degraded by $\sim 8\%$ in the course of 5 h. For comparison CuO commercial powder was also assessed for catalytic activity with RB aqueous solution, but the RB was degraded by only 14% in the presence of CuO commercial powder (figure 5e). The degradation of RB in the presence of CuO flowers and petals is shown in figure 5a and b, respectively. RB was $\sim 85\%$ and 81% degraded after 5 h in the presence of CuO

petals and flowers, respectively. This demonstrates that the CuO petals are more efficient in degrading RB compared to CuO flowers and commercial CuO powder.

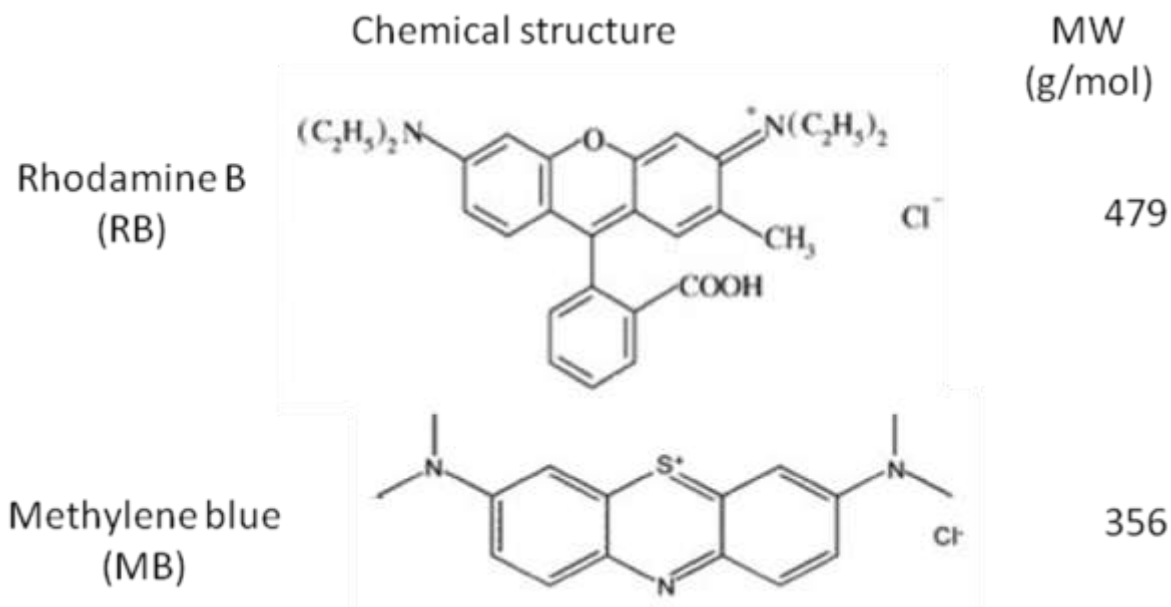


Figure 4: The structural diagram of RB and MB dyes.

Possible reasons for the high efficiency of CuO petals compared to CuO flowers can be attributed to their specific surface area. CuO petals have larger surface area $8.4 \text{ m}^2/\text{g}$ as compared to the CuO flowers $5.5 \text{ m}^2/\text{g}$ and commercial CuO powder $1.7 \text{ m}^2/\text{g}$, which may enable petals have more active surface sites compared to the CuO flowers explaining the faster degradation of the RB when CuO petals are used. Another possibility for the faster CuO petals response is based on the dissociation of water on the CuO NSs surface. It is well known that metal oxides grown by chemical bath method have excess oxygen vacancies in their grown structures. The CuO grown by this method may contain excess oxygen vacancies. Schaub R and

coworkers studied the dissociation of water on oxygen vacancies in rutile phase TiO_2 . The water adsorbs dissociatively in oxygen vacancies and via proton transfer to a neighboring bridging oxygen atom creating two bridging hydroxyl groups per initial vacancy. So we expect that the oxygen vacancies act as active sites for water dissociation on CuO NSs. The reason for the large reactivity of the vacancies is associated with the high energy of the defects [27, 28]. CuO petals may contain more oxygen vacancies in their structure and produces more hydroxyl ions which are one of the active species to degrade MB and RB dyes.

3.2.2 Catalytic activity in methylene blue

To confirm our results, we used another more stable organic dye, methylene blue (MB), to study the catalytic activity of the CuO petals and flowers-like NSs. The amounts of MB, H_2O_2 , and CuO NSs were kept fixed as mentioned above and the chemical structure of the MB dye is shown in figure 4. The absorption curve of the MB with a maximum peak at ~ 664 nm was used to evaluate the degradation process of MB.

The catalytic process was again observed via UV-visible spectroscopy. At similar chosen reaction intervals as for the RB, and since the MB is known to be more stable compared to the RB, the catalytic reaction was allowed to continue for 24 h to completely degrade the MB

The typical UV-visible spectra of the degradation of the MB aqueous solution are shown in figure 5 c and d. The catalytic performance of the MB+ H_2O_2 system was measured as before, and the MB was degraded by $\sim 28\%$ in the course of 24 h when only H_2O_2 was added to the MB solution. This demonstrates that without the addition of any CuO NSs, the MB is degraded in the presence of H_2O_2 but with less change in short time. MB degradation was also examined in the presence of commercial CuO powder, and it was found to be degraded by 55% after 24 h. The

MB was almost 95% degraded in the presence of CuO petals, while it was ~ 72% degraded when CuO flowers were applied in the aqueous solution of MB+H₂O₂. The CuO petals were again found more efficient in comparison to CuO flowers and commercial CuO powder, and the reason might be same as discussed above. Since more of the MB molecules and H₂O₂ can be adsorbed on the surface of the CuO petals and consequently, more hydroxyl radicals will be generated, and destructively oxidizes the MB dye, as discussed below [29].

Previously H₂O₂ has been used for the oxidative degradation of organic dye; however the more stable MB dye is much more resistant to H₂O₂ oxidizer [30]. The combination of H₂O₂ and metal oxides catalysts with the ability to form reduction and oxidation pairs has been used to degrade the organic compounds [31]. The catalytic decomposition of H₂O₂ generates free radical species like HO•, HOO•, or O₂•⁻, and these species, especially the HO•, are the leading oxidation agent; that is to say, they are more dominant than H₂O₂. These species are responsible for the efficient degradation of organic dyes [32]. The CuO petals- and flowers-like NSs may play the critical role of decomposing H₂O₂, and producing the free radical species as HO•, HOO•, or O₂•⁻, that are responsible for degrading the MB molecules. However, the formation of free radical pairs is the key factor in the remarkable catalytic degradation of MB by the CuO NSs compared to that for the CuO commercial powder.

The main process in the degradation of MB is the adsorption–oxidation–desorption mechanism as discussed by Zhang et al. for MnO₂ [29]. The MB molecule and H₂O₂ were first adsorbed on the surface of the nanostructures, and then free radical species of HO•, HOO•, or O₂•⁻ were produced by the catalytic decomposition of H₂O₂. These free radicals cause the destructive oxidation of the organic dye. The catalyst recovers immediately after desorption of the degraded dye molecules that have left the nanostructure surface [33]. In addition, comparing

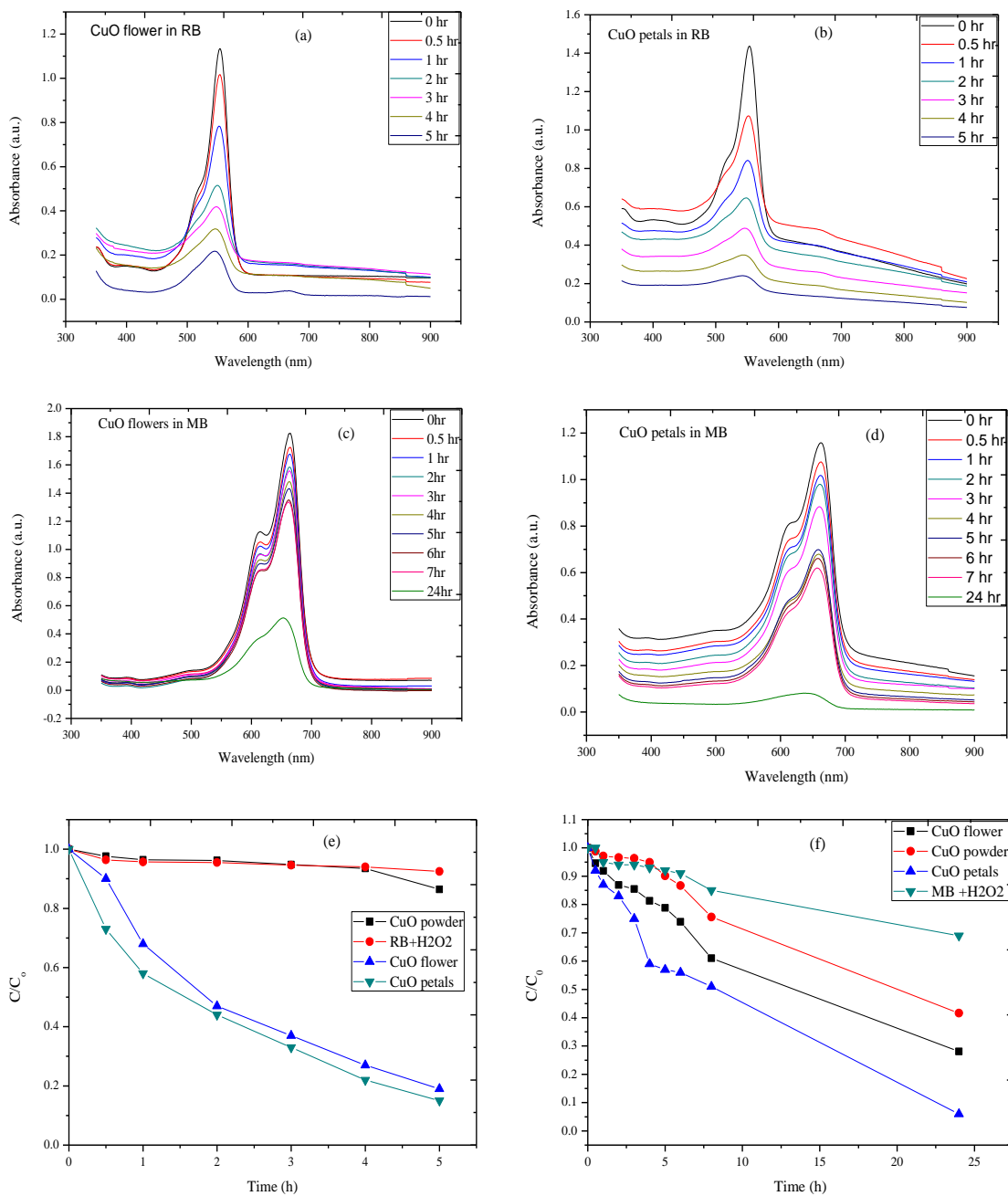


Figure 5: (a-d) UV- visible absorption spectral changes of an aqueous solution of RB and MB in presence of CuO flowers and petals, and H₂O₂.(e, f) Plots of the concentration ratio of RB and MB in an aqueous solution against specific time intervals in the presence or absence of CuO.

MB with RB dye, CuO NSs have a relatively strong catalytic response in the case of RB, as shown in figure 5e and 5f. RB takes only 5 h to completely degrade while MB degraded after 24 h under the same conditions. The RB has a large molecular size compared to the MB dye and due to this larger size more free radicals can react with RB and degrade it faster. The other possible reason is that the RB molecules contain additional end carboxyl groups that may effectively anchor onto the CuO surface, which in turns enhances adsorption of the RB compared to MB [26, 34].

The kinetics of degradation was studied for the RB and MB dyes. The degradation reactions of all CuO NSs with both dyes exhibited pseudo-first-order kinetics model with respect to the degradation time. The results were nearly consistent with the liner equation [35].

$$\ln(C/C_0) = -kt$$

Where C_0 is the initial concentration of a dye and C is the concentration at time t , k is the reaction constant of the first-order reaction. For the first order kinetics, a plot of $\ln(C/C_0)$ vs. time for RB and MB degradation using CuO petals is illustrated in figure 6, while the plots of CuO flowers and commercial powder were not shown here. The figure 6a and b represents a good linear correlation (R^2), suggesting that the degradation reaction follows the first-order kinetics with respect to both MB and RB. The slope of the linear line gives the first order rate constant and were estimated to be 0.022 h^{-1} (commercial CuO), 0.33 h^{-1} (CuO flower) and 0.359 h^{-1} (CuO petals) for RB, and 0.037 h^{-1} (commercial CuO), 0.052 h^{-1} (CuO flower) and 0.115 h^{-1} (CuO petals), respectively for MB. This indicates that for both dyes the degradation rates follow the order of CuO petals > CuO flowers > CuO commercial powder. The catalytic activity of CuO petals are higher than CuO flowers for both dyes, and the higher rate constant for RB confirms our previous discussion about the fast degradation of RB compared to that of the MB.

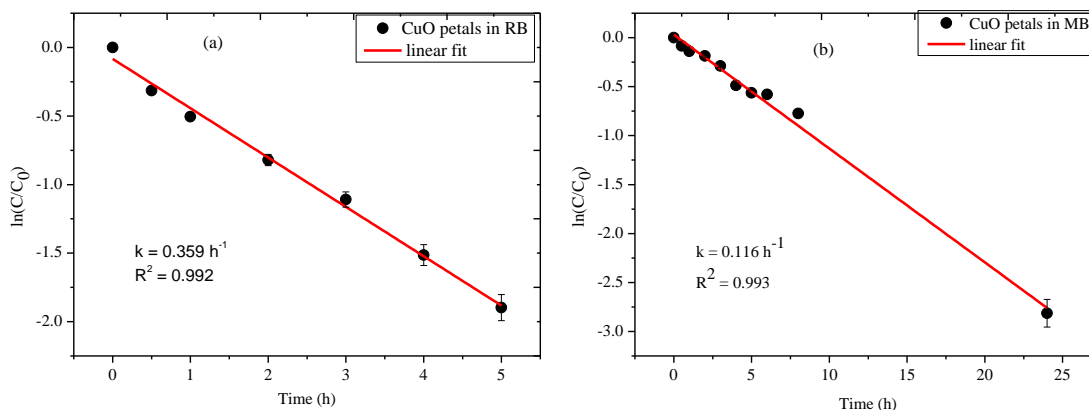


Figure 6: First-order kinetic plot of $\ln(C_0/C)$ vs. time of (a) RB degradation and (b) MB degradation in presence of CuO petals.

To check the reusability of the CuO NSs as a catalyst, we collected the CuO petals after the degradation process then we thoroughly washed them with DI water, and left them to dry at room temperature. The collected CuO petals have the same weight as when was used in the first catalytic reaction. The collected CuO petals were put in the MB solution in combination with the H_2O_2 using the same procedure as discussed above. The degradation of the MB was observed with UV-visible spectra for the first 5 h and it showed 35% degradation (not shown here), while in comparison with that for the fresh CuO petals it was 45% during this time. We can predict from this result that the CuO petals are reusable.

4. Conclusion

In conclusion, CuO petals- and flowers-like nanostructures were used to degrade the two commercial organic dyes, MB and RB. The degradation of the MB and the RB in the presence of H_2O_2 shows a strong catalytic effect of the CuO NSs. The CuO petals show stronger catalytic activity in comparison of the degradation of the organic dyes with that of flowers like CuO NSs.

The possible reasons are the higher specific surface area of CuO petals. These CuO NSs have the potential to be used as a room temperature catalyst without using any specific light source.

Acknowledgement

We acknowledge the partial financial support from the Advanced Functional Materials (AFT) grant at Linköping University, Sweden and from the MUST University AJK, Pakistan. We thank Dr. Amir for conducting specific surface area measurements.

References:

- [1] S. Rackauskas, A.G. Nasibulin, H. Jiang, Y. Tian, V.I. Kleshch, J. Sainio, E.D. Obraztsova, S.N. Bokova, A.N. Obraztsov, E. Kauppinen, *Nanotechnology* 20 (2009) 165603.
- [2] R. Pratima, K.A. Solanki, V.A. Ved, B.D. Malhotra, *NPG Asia Mater.* 3 (2011) 17-24.
- [3] M. Yin, C.K. Wu, Y.B. Lou, C. Burda, J.T. Koberstein, Y.M. Zhu, S. O'Brien, *J. Am. Chem. Soc.* 127 (2005) 9506-9511.
- [4] D. Li, J. Hu, R. Wu, J.G. Lu, *Nanotechnology* 21 (2010) 485502.
- [5] Y. Xu, D. Chen, X. Jiao, *J. Phys. Chem. B* 109 (2005) 13561-13566.
- [6] S. Venkatachalam, H.W. Zhu, C. Masarapu, K.H. Hung, Z. Liu, K. Suenaga, B.Q. Wei, *ACS Nano* 3 (2009) 2177-2184.
- [7] C.T. Hsieh, J.M. Chen, H.H. Lin, H.C. Shih, *Appl. Phys. Lett.* 83 (2003) 3383-3385.
- [8] J. Huang, S.R. Wang, Y.Q. Zhao, X.Y. Wang, S.P. Wang, S.H. Wu, S.M. Zhang, W.P. Huang, *Catal. Commun.* 7 (2006) 1029-1034.
- [9] D.P. Singh, A.K. Ojha, O.N. Srivastava, *J. Phys. Chem. C* 113 (2009) 3409-3418.
- [10] Y. Liu, Y. Chu, Y.J. Zhuo, M.Y. Li, L.L. Li, L.H. Dong, *Cryst. Growth & Des.* 7 (2007) 467-470.
- [11] H.H. Wang, Q. Shen, X.P. Li, F.L. Liu, *Langmuir* 25 (2009) 3152-3158.
- [12] Y. Zhao, J. Zhao, Y. Li, D. Ma, S. Hou, L. Li, X. Hao, Z. Wang, *Nanotechnology* 22 (2011) 115604.
- [13] M.H. Cao, C.W. Hu, Y.H. Wang, Y.H. Guo, X. Guo, E.B. Wang, *Chem. Commun.* 15 (2003) 1884-1885.

- [14] L. Armelao, D. Barreca, M. Bertapelle, G. Bottaro, C. Sada, E. Tondello, *Thin Solid Films* 442 (2003) 48-52.
- [15] J.T. Zhang, J.F. Liu, Q. Peng, X. Wang, Y.D. Li, *Chem. Mater.* 18 (2006) 867-871.
- [16] H. Zhang, X. Zhang, H. Li, Z. Qu, S. Fan, M. Ji, *Cryst. Growth & Des.* 7 (2007) 820-825.
- [17] M.A. Kanjwal, M.A.N. Barrakat, F.A. Sheikh, S.J. Park, H.Y. Kim, *Macromolecular Rese/arch* 18 (2010) 233-240.
- [18] S.F. Yin, B.Q. Xu, C.F. Ng, C.T. Au, *Appl. Catal. B: Environ.* 48 (2004) 237-241.
- [19] S. Malato, J. Blanco, A. Vidal, C. Richter, *Appl. Catal. B: Environ.* 37 (2002) 1-15.
- [20] A. Nezamzadeh-Ejchieh, S. Hushmandrad, *Appl. Catal. A* 388 (2010) 149-159.
- [21] K. Zhou, R. Wang, B.L. Xu, *Nanotechnology* 17 (2006) 3939-3943.
- [22] R. Narayanan, A. El-Sayed Mostafa, *Nano Lett* 4 (2004) 1343-1348.
- [23] M. Vaseem, A. Umar, H. Kim, Y-B. Hahn, *J. Phys. Chem. C* 112 (2008) 5729-5735.
- [24] Z. Zhang, H. Sun, X. Shao, D. Li, H. Yu, M. Han, *Adv. Mater.* 17 (2005) 42-47.
- [25] J. Liu, X. Huang, Y. Li, K.M. Suleiman, X. He, F. Sun, *Cryst. Growth & Des.* 6 (2006) 1690-1696.
- [26] K. Zhang, Ze-Da Meng, W-C Oh, *J. Korean Ceramic Society* 47 (2010) 169-176.
- [27] R. Schaub, P. Thostru, N. Lopez, E. Lægsgaard, I. Stensgaard, J.K. Nørskov, F. Besenbacher, *Physical Rev. Lett.* 87 (2001) 2661041-2661044.
- [28] S. Warren, W.R. Flavell, A.G. Thomas, J. Hollingworth, P.M. Dunwoody, S. Downes, C. Changkang, *Surface Science* 436 (1999) 1-8.
- [29] W. Zhang, Z. Yang, X. Wang, Y. Zhang, X. Wen, S. Yang, *Catal. Commun.* 7 (2006) 408-412.

- [30] K.M. Thompson, W.P. Griffith, M. Spiro, *J. Chem. Soc. Chem. Commun.* 21 (1992) 1600-1601.
- [31] W.X. Zhang, H. Wang, Z.H. Yang, F. Wang, *Colloids Surf. A* 304 (2007) 60-64.
- [32] X. Peng, I. Izumi, *Nanotechnology* 22 (2011) 01570.
- [33] H. Zhang, J. Feng, M. Zhang, *Materials Research Bulletin* 43 (2008) 3221-3226.
- [34] X-M. Song, J-M. Wu, M. Yan, *Thin Solid Films* 517 (2009) 4341-4347.
- [35] A. Mehrdad, B. Massoumi, R. Hashemzadeh, *Chem. Eng. J.* 168 (2011) 1073-1078.